A prefusion SARS-CoV-2 spike RNA vaccine is highly immunogenic and prevents lung infection in non-human primates

Authors

Annette B. Vogel[1#], Isis Kanevsky[2#], Ye Che[3], Kena A. Swanson[2], Alexander Muik[1], Mathias Vormehr[1], Lena M. Kranz[1], Kerstin C. Walzer[1], Stephanie Hein[1], Alptekin Güler[1], Jakob Loschko[2], Mohan S. Maddur[2], Kristin Tompkins[2], Journey Cole[4], Bonny G. Lui[1], Thomas Ziegenhals[1], Arianne Plaschke[1], David Eisel[1], Sarah C. Dany[1], Stephanie Fesser[1], Stephanie Erbar[1], Ferdia Bates[1], Diana Schneider[1], Bernadette Jesionek[1], Bianca Sänger[1], Ann-Kathrin Wallisch[1], Yvonne Feuchter[1], Hanna Junginger[1], Stefanie A. Krumm[1], André P. Heinen[1], Petra Adams-Quack[1], Julia Schlereth[1], Christoph Kröner[1], Shannan Hall-Ursone[4], Kathleen Brasky[4], Matthew C. Griffor[3], Seungil Han[3], Joshua A. Lees[3], Ellene H. Mashalidis[3], Parag V. Sahasrabudhe[3], Charles Y. Tan[2], Danka Pavliakova[2], Guy Singh[2], Camila Fontes-Garfias[5], Michael Pride[2], Ingrid L. Scully[2], Tara Ciolino[2], Jennifer Obregon[2], Michal Gazi[6], Ricardo Carrion, Jr.[4], Kendra J. Alfson[6], Warren V. Kalina[2], Deepak Kaushal[4], Pei-Yong Shi[5], Thorsten Klamp[1], Corinna Rosenbaum[1], Andreas N. Kuhn[1], Özlem Türeci[1], Philip R. Dormitzer[2], Kathrin U. Jansen[2], Ugur Sahin[1,7]

\# Contributed equally

Affiliations:
[1] BioNTech, An der Goldgrube 12, 55131 Mainz, Germany;
[2] Pfizer, 401 N. Middletown Rd., Pearl River, NY 10965, United States;
[3] Pfizer, 280 Shennecossett Rd., Groton, CT 06340, United States;
[4] Southwest National Primate Research Center, Texas Biomedical Research Institute, 8715 W. Military Dr, San Antonio, TX 78227, United States;
[5] University of Texas Medical Branch, 301 University Blvd, Galveston, TX 77555, United States;
[6] Texas Biomedical Research Institute, 8715 W Military Dr, San Antonio, TX 78227, United States;
[7] TRON gGmbH – Translational Oncology at the University Medical Center of the Johannes Gutenberg University, Freiligrathstraße 12, 55131 Mainz, Germany;

Correspondence: Prof. Dr. Ugur Sahin**,** BioNTech SE, An der Goldgrube 12, 55131 Mainz, Germany, Tel: +49 6131 2161 201; Email: Ugur.Sahin@biontech.de

Abstract

To contain the coronavirus disease 2019 (COVID-19) pandemic, a safe and effective vaccine against the new severe acute respiratory syndrome coronavirus-2 (SARS-CoV-2) is urgently needed in quantities sufficient to immunise large populations. In this study, we report the design, preclinical development, immunogenicity and anti-viral protective effect in rhesus macaques of the BNT162b2 vaccine candidate. BNT162b2 contains an LNP-formulated nucleoside-modified mRNA that encodes the spike glycoprotein captured in its prefusion conformation. After expression of the BNT162b2 coding sequence in cells, approximately 20% of the spike molecules are in the one-RBD 'up', two-RBD 'down' state. Immunisation of mice with a single dose of BNT162b2 induced dose level-dependent increases in pseudovirus neutralisation titers. Prime-boost vaccination of rhesus macaques elicited authentic SARS-CoV-2 neutralising geometric mean titers 10.2 to 18.0 times that of a SARS-CoV-2 convalescent human serum panel. BNT162b2 generated strong T_H1 type $CD4^+$ and $IFN\gamma^+$ $CD8^+$ T-cell responses in mice and rhesus macaques. The BNT162b2 vaccine candidate fully protected the lungs of immunised rhesus macaques from infectious SARS-CoV-2 challenge. BNT162b2 is currently being evaluated in a global, pivotal Phase 2/3 trial (NCT04368728).

52 # Main

53 ## Introduction

54 Due to the shattering impact of the coronavirus disease 2019 (COVID-19) pandemic on human

55 health and society, multiple collaborative research programs have been launched, leading to

56 new insights and progress towards vaccine development. Soon after it emerged in December

57 2019, severe acute respiratory syndrome coronavirus-2 (SARS-CoV-2) was identified as a β-

58 coronavirus with high sequence similarity to bat-derived SARS-like coronaviruses[1,2]. The

59 globalised response is mirrored by the upload of over 92,000 viral genome sequences as of

60 August 29, 2020, to GISAID (Global Initiative on Sharing All Influenza Data).

61 The trimeric spike glycoprotein (S) of SARS-CoV-2 binds its cellular receptor, angiotensin

62 converting enzyme 2 (ACE2), through a receptor-binding domain (RBD), which is part of its

63 N-terminal furin cleavage fragment (S1)[3,4]. S rearranges to translocate the virus into cells by

64 membrane fusion[5,6]. The C-terminal furin cleavage fragment (S2) contains the fusion

65 machinery[7]. Membrane fusion can be blocked by mutating S residues 986 and 987 to prolines,

66 producing an S antigen stabilised in the prefusion conformation (P2 S)[8–10]. The RBD is a key

67 target for virus neutralising antibodies, with an 'up' conformation, in which more neutralising

68 epitopes are exposed, and a 'down' conformation in which many epitopes are buried[5,10–12]. In

69 addition, some neutralising antibodies bind S epitopes outside the RBD.

70 During this pandemic, fast vaccine availability is critical. COVID-19 vaccine candidates based

71 on different platforms are already in clinical trials, with the most advanced based on viral vector

72 and nucleic acid technologies[13–16]. We report the preclinical development of BNT162b2, a lipid-

73 nanoparticle (LNP) formulated N^1-methyl-pseudouridine (m1Ψ) nucleoside-modified mRNA

74 (modRNA) vaccine candidate that encodes P2 S with a native furin cleavage site resulting in

75 the S1 and S2 cleavage fragments (Fig. 1a). The m1Ψ-modification dampens innate immune

76 sensing, and, together with optimised non-coding sequence elements, increases RNA

77 translation *in vivo*[17–19]. ModRNA vaccines have already proven immunogenic for several viral

78 targets[20,21]. BNT162b2 has been evaluated in phase 1 clinical trials in the US (NCT04368728)

79 and Germany (NCT04380701, EudraCT: 2020-001038-36), and is now being evaluated in a

80 pivotal, global, phase 2/3 safety and efficacy study[15].

81   **Results**

82   BNT162b2 RNA *in vitro* transcribed by T7 polymerase from a plasmid DNA template has a

83   single, sharp-peak microfluidic capillary electrophoresis profile, consistent with its calculated

84   length of 4,283 nucleotides, indicating purity and integrity (Fig. 1b). When HEK293T/17 cells

85   were incubated with BNT162b2 (which is LNP-formulated) or with BNT162b2 RNA mixed

86   with a transfection reagent, robust expression of P2 S was detectable by flow cytometry

87   (Extended Data Fig. 1a).

88   For structural characterisation, P2 S was expressed in Expi293F cells from DNA that encodes

89   the same amino acid sequence as BNT162b2 RNA, with the addition of a C-terminal TwinStrep

90   tag for affinity purification. The trimeric P2 S bound the human ACE2 peptidase domain (PD),

91   and an anti-RBD human neutralising antibody B38 with high affinity (K_D 1 nM, Extended Data

92   Fig. 1b,c)[22]. Structural analysis by cryo-electron microscopy (cyro-EM) produced a 3.29 Å

93   nominal resolution mass density map, into which a previously published atomic model[10] was

94   fitted and rebuilt (Fig. 1c,d; Extended Data Fig. 2, Extended Data Table 1). The rebuilt model

95   shows good agreement with reported structures of prefusion full-length wild type S and its

96   ectodomain with P2 mutations[5,10]. Three-dimensional classification of the dataset showed a

97   class of particles that was in the one RBD 'up' (accessible for receptor binding), two RBD

98   'down' (closed) conformation and represented 20.4% of the trimeric molecules. The remainder

99   were in the all RBD 'down' conformation (Fig. 1e, Extended Data Fig. 2c). The RBD in the

100 'up' conformation was less well resolved than other parts of the structure, suggesting

101 conformational flexibility and a dynamic equilibrium between RBD 'up' and RBD 'down'

102 states as also suggested by others[5,23]. Nevertheless, the binding and structural analyses indicate

103 that the BNT162b2 RNA sequence encodes a recombinant P2 S that authentically presents the

104 ACE2 binding site and other epitopes targeted by SARS-CoV-2 neutralising antibodies.

105 To characterise BNT162b2-elicited B- and T-cell responses, BALB/c mice were immunized

106 intramuscularly (IM) once with 0.2, 1, or 5 µg BNT162b2 or received a buffer control. S1- and

107 RBD-binding serum IgG developed rapidly at all dose levels in a dose-dependent manner. For

108 S1-binding antibodies, the geometric mean concentration (GMC) in the 5 µg group was 386

109 µg/mL at Day 28 (Fig. 2a, Extended Data Fig. 3a). At Day 28 after immunisation, vaccine-

110 elicited IgG had a strong binding affinity for S1 (geometric mean K_D 12 nM) and the RBD

111 (geometric mean K_D 0.99 nM), with both having a low off-rate (Extended Data Fig. 3b). SARS-

112 CoV-2 neutralising activity in mouse serum was measured by a vesicular stomatitis virus

113 (VSV)-based SARS-CoV-2 pseudovirus neutralisation assay. Fifty percent pseudovirus
114 neutralisation geometric mean titers (pVNT$_{50}$ GMTs) increased steadily after immunisation to
115 26, 176, and 296 on Day 28 for the 0.2, 1, and 5 µg dose levels, respectively (Fig. 2b, Extended
116 Data Fig. 3c).

117 A high fraction of splenocytes of CD4$^+$ and CD8$^+$ T-cell phenotype isolated from mice on Days
118 12 and 28 after BNT162b2-immunisation had a strong antigen-specific IFNγ and IL-2 response
119 in ELISpot and intracellular cytokine staining flow cytometry analysis when re-stimulated *ex*
120 *vivo* with a full-length S peptide pool (Fig. 2c-e). Total splenocytes harvested on Day 28 and
121 *ex vivo* re-stimulated with the full-length S peptide pool secreted high levels of the T$_H$1
122 cytokines IL-2 or IFNγ, but minute amounts of the T$_H$2 cytokines IL-4, IL-5 and IL-13 as
123 measured in multiplex immunoassays (Fig. 2f).

124 BNT162b2-induced effects on proliferation and dynamics of immune cell populations were
125 assessed in injection site draining lymph nodes (dLNs), which are the principal immune-
126 educated compartments for proficient T- and B-cell priming, and in blood and spleen for
127 evaluation of its systemic effects. Higher numbers of plasma cells, class switched IgG1- and
128 IgG2a-positive B cells, and germinal center B cells were observed in dLNs and spleens of mice
129 12 days after immunisation with 5 µg BNT162b2 than after immunisation with buffer
130 (Extended Data Fig. 4a, b). In Day 7 post-immunisation blood, there were significantly fewer
131 circulating B cells than in blood from buffer-immunised mice (Extended Data Fig. 4c), which
132 may imply that B-cell homing to lymphoid compartments augments B cell counts in dLN and
133 spleen. The dLNs from BNT162b2-immunised mice also have significantly elevated counts of
134 CD8$^+$ and CD4$^+$ T cells, which was most pronounced for T follicular helper (T$_{FH}$) cells,
135 including ICOS$^+$ subsets essential for germinal center formation (Extended Data Fig. 4a)[24].
136 BNT162b2 immunisation increased CD8$^+$ T cell counts in the blood and T$_{FH}$ cell counts in the
137 spleen and blood (Extended Data Fig. 4b, c). These data indicate that BNT162b2 concurrently
138 elicits strong SARS-CoV-2 pseudovirus neutralising titers and systemic T$_H$1-driven CD4$^+$ and
139 CD8$^+$ T-cell responses.

140 To assess BNT162b2-mediated protection in non-human primates, groups of six male, 2-4 year
141 old rhesus macaques were immunised IM with 30 or 100 µg of BNT162b2 or saline control on
142 Days 0 and 21. S1-binding IgG was readily detectable by Day 21 after Dose 1, and levels
143 increased further after Dose 2 through Day 28 (Fig. 3a). Seven days after Dose 2 (Day 28), the
144 GMCs of S1-binding IgG were 30,339 units (U)/mL (30 µg dose level) and 34,668 U/mL

145   (100 µg dose level). For comparison, the S1-binding IgG GMC of a panel of 38 SARS-CoV-2

146   convalescent human sera was 631 U/mL, substantially lower than the GMCs of the immunised

147   rhesus macaques after one or two doses.

148   Fifty percent virus neutralisation GMTs, measured by an authentic SARS-CoV-2 neutralisation

149   assay[25], were detectable in rhesus macaque sera by Day 21 after Dose 1 and peaked at a GMT

150   of 962 (Day 35, 14 days after Dose 2 of 30 µg) or 1,689 (Day 28, 7 days after Dose 2 of 100 µg;

151   Fig. 3b). Robust GMTs of 285 for 30 µg and 310 for 100 µg dose levels persisted to at least

152   Day 56 (most recent time point tested). For comparison, the neutralisation GMT of the human

153   convalescent serum panel was 94.

154   S-specific T-cell responses were analysed in BNT162b2-immunised rhesus macaques and

155   saline-immunised controls by ELISpot and intracellular cytokine staining (ICS). Peripheral

156   blood mononuclear cells (PBMCs) were collected before immunisation and at the times

157   indicated after Doses 1 and 2. Strong IFNγ but minimal IL-4 responses were detected by

158   ELISpot after Dose 2 (Fig. 3c,d, Extended Data Fig. 5). ICS confirmed that BNT162b2 elicited

159   strong S-specific IFNγ producing T-cell responses, including a high frequency of CD4$^+$ T cells

160   that produced IFNγ, IL-2, and TNF but a low frequency of CD4$^+$ T cells that produced IL-4,

161   indicating a T_H1-biased response (Fig. 3e,f). BNT162b2 also elicited S-specific

162   IFNγ$^+$ producing CD8$^+$ T cells (Fig. 3g).

163   Six rhesus macaques that had received two immunisations with 100 µg BNT162b2 and three

164   age-matched macaques that had received saline were challenged 55 days after Dose 2 with

165   1.05×10^6 plaque forming units of SARS-CoV-2 (strain USA-WA1/2020), split equally

166   between intranasal and intratracheal routes, as previously described[26]. Three additional non-

167   immunised, age-matched rhesus macaques (sentinels) were mock-challenged with cell culture

168   medium. Nasal and oropharyngeal (OP) swabs were collected and bronchoalveolar lavage

169   (BAL) was performed at the times indicated, and samples were tested for SARS-CoV-2 RNA

170   (genomic RNA or subgenomic transcripts) by reverse-transcription quantitative polymerase

171   chain reaction (RT-qPCR; Fig. 4). All personnel performing clinical, radiological,

172   histopathological, or RT-qPCR evaluations were blinded to the group assignments of the

173   macaques.

174   Viral RNA was detected in BAL fluid from 2 of the 3 control-immunised macaques on Day 3

175   after challenge and from 1 of 3 on Day 6 (Fig. 4a). At no time point sampled was viral RNA

176   detected in BAL fluid from the BNT162b2-immunised and SARS-CoV-2 challenged macaques
177   (Fig. 4a). The difference in viral RNA detection in BAL fluid between BNT162b2-immunised
178   and control-immunised rhesus macaques after challenge is highly statistically significant (by a
179   nonparametric test, p=0.0014).

180   From control-immunised macaques, viral RNA was detected in nasal swabs obtained on Days
181   1, 3, and 6 after SARS-CoV-2 challenge; from BNT162b2-immunised macaques, viral RNA
182   was detected only in nasal swabs obtained on Day 1 after challenge and not in swabs obtained
183   on Day 3 or subsequently (Fig. 4b). The pattern of viral RNA detection from OP swabs was
184   similar to that for nasal swabs (Fig. 4c).

185   In general, virus-challenged animals showed no clinical signs of significant disease. We
186   conclude that the 2-4 year old male rhesus macaque challenge model is primarily a SARS-CoV-
187   2 infection model and not a COVID-19 disease model.

188   **Discussion**
189   We demonstrate that BNT162b2, an LNP-formulated, m1Ψ nucleoside-modified mRNA
190   encoding SARS-CoV-2 S captured in a prefusion conformation is highly immunogenic in mice
191   and rhesus macaques. Expression from DNA of protein with the BNT162b2-encoded amino
192   acid sequence confirmed the P2 S prefusion conformation by cryo-EM. This analysis confirmed
193   that the antigenically important RBD can assume the 'up' conformation, with the receptor
194   binding site, rich in neutralising epitopes, accessible in a proportion of the molecules[27]. The
195   alternative states observed likely reflect a dynamic equilibrium between RBD 'up' and 'down'
196   positions[10,23]. Binding of expressed and purified P2 S to ACE2 and a neutralising monoclonal
197   antibody further demonstrates its conformational and antigenic integrity.

198   In mice, a single injection of BNT162b2 elicited high neutralizing titers and strong T_H1 and T_{FH}
199   type $CD4^+$ and $IFN\gamma^+IL-2^+$ $CD8^+$ T-cell responses. Both BNT162b2 induced $CD4^+$ T-cell types
200   may support antigen-specific antibody generation and maturation, and potentially protection
201   from infectious challenge. Limitation and clearance of virus infection is promoted by the
202   interplay of neutralising antibodies with $CD8^+$ T cells that eliminate intracellular virus
203   reservoirs. $CD8^+$ T cells may also reduce the influx of monocytes into infected lung tissue,
204   which can be associated with undesirable IL-6 and TNF production and impaired antigen
205   presentation[28,29]. The contributions of the immune effector systems to human protection from

206   SARS-CoV-2 is not yet understood. Therefore, it appears prudent to develop COVID-19

207   vaccines that enlist concomitant cognate B cell, $CD4^+$ T cell, and $CD8^+$ T-cell responses.

208   The immunogenicity of BNT162b2 in rhesus macaques paralleled its immunogenicity in mice.

209   Seven days after Dose 2 of 100 μg, the neutralising GMT reached 18-times that of a human

210   SARS-CoV-2 convalescent serum panel and remained 3.3-times higher than this benchmark

211   five weeks after the last immunisation. The strongly T_H1-biased $CD4^+$ T-cell response and

212    $IFN\gamma^+$ $CD8^+$ T-cell response to BNT162b2 is a pattern favoured for vaccine safety and efficacy,

213   providing added reassurance for clinical translation[30]. BNT162b2 protected 2-4 year old rhesus

214   macaques from infectious SARS-CoV-2 challenge, with reduced detection of viral RNA in

215   immunised animals compared to those that received saline and with no evidence of clinical

216   exacerbation. Strong RT-qPCR evidence for lower respiratory tract protection was

217   demonstrated by the absence of detectable SARS-CoV-2 RNA in serial BAL samples obtained

218   starting 3 days after challenge of BNT162b2-immunised rhesus macaques.

219   We recently presented data from immunisation with BNT162b1, a vaccine candidate that has

220   the same LNP-formulated m1Ψ nucleoside-modified RNA platform but expresses a trimerised,

221   secreted RBD (Vogel et al., manuscript in preparation). The pattern, magnitude and durability

222   of humoral and cellular responses to BNT162b1 in mice and macaques were in the range of

223   those elicited by BNT162b2, as was protection of macaques from virus challenge, indicating

224   that these features are largely class-intrinsic for this particular vaccine platform. BNT162b1

225   elicits high SARS-CoV-2 neutralizing titers and strong T_H1-biased $CD4^+$ and $IFN\gamma^+$ and $IL-2^+$

226    $CD8^+$ T cell responses in humans, consistent with the preclinical findings[15,31,32].

227   The selection of BNT162b2 over BNT162b1 for further clinical testing was largely driven by

228   greater tolerability of BNT162b2 with comparable immunogenicity in clinical trials[15] and the

229   broader range of T-cell epitopes on the much larger full length spike. A global, pivotal, phase

230   3 safety and efficacy study of immunisation with BNT162b2 (NCT04368728) is now well

231   under way and may answer those open questions that cannot be addressed by preclinical

232   models.

233

Materials and Methods

Ethics statement.

All mouse studies were performed at BioNTech SE, and protocols were approved by the local authorities (local welfare committee), conducted according to FELASA recommendations and in compliance with the German Animal Welfare Act and Directive 2010/63/EU. Only animals with an unobjectionable health status were selected for testing procedures.

Immunisations for the non-human primate (NHP) study were performed at the University of Louisiana at Lafayette-New Iberia Research Center (NIRC), which is accredited by the Association for Assessment and Accreditation of Laboratory Animal Care (AAALAC, Animal Assurance #: 000452). The work was in accordance with USDA Animal Welfare Act and Regulations and the NIH Guidelines for Research Involving Recombinant DNA Molecules, and Biosafety in Microbiological and Biomedical Laboratories. All procedures performed on these animals were in accordance with regulations and established guidelines and were reviewed and approved by an Institutional Animal Care and Use Committee or through an ethical review process. Infectious SARS-CoV-2 challenge for the NHP study was performed at the Southwest National Primate Research Center. Animal husbandry followed standards recommended by AAALAC International and the NIH Guide for the Care of Use of Laboratory Animals. This study was approved by the Texas Biomedical Research Institute Animal Care and Use Committee.

Protein and peptide reagents.

Purified recombinant SARS-CoV-2 S1 subunit including a histidine tag and the RBD tagged with the Fc region of human IgG1 (both Sino Biological) were used in ELISA to detect SARS-CoV-2 S-specific IgG in mice. Purified recombinant SARS-CoV-2 S1 and RBD with a histidine tag (both Sino Biological) were used for surface plasmon resonance (SPR) spectroscopy. An overlapping 15-mer peptide pool of the S protein was used for ELISpot, cytokine profiling and intracellular cytokine staining. An irrelevant peptide control (SPSYVYHQF, derived from gp70 AH-1[33]) or a CMV peptide pool was used as control for ELISpot assays. All peptides were obtained from JPT Peptide Technologies.

262 **Human convalescent sera.**

263 Human COVID-19 convalescent sera (n=38) were drawn from donors 18-83 years of age at

264 least 14 days after PCR-confirmed diagnosis and at a time when the participants were

265 asymptomatic. Serum donors had symptomatic infections (35/38), or had had been hospitalised

266 (1/38). Sera were obtained from Sanguine Biosciences (Sherman Oaks, CA), the MT group

267 (Van Nuys, CA) and Pfizer Occupational Health and Wellness (Pearl River, NY) and used

268 across different studies as reference benchmark.

269 **Cell culture.**

270 Human embryonic kidney (HEK)293T/17 and Vero 76 cells (both ATCC) were cultured in

271 Dulbecco's modified Eagle's medium (DMEM) with GlutaMAX™ (Gibco) supplemented with

272 10% fetal bovine serum (FBS [Sigma-Aldrich]). Cell lines were tested for mycoplasma

273 contamination after receipt, before expansion and cryopreservation. For studies including NHP

274 samples, Vero 76 and Vero CCL81 (both ATCC) cells were cultured in DMEM (Gibco)

275 containing 2% HyClone fetal bovine and 100 U/mL penicillium/streptomycin (Gibco).

276 Expi293F™ cells were grown in Expi293™ media and transiently transfected using

277 ExpiFectamine™293 (all from Thermo Fisher Scientific).

278 ***In vitro* transcription and purification of RNA.**

279 To generate the template for RNA synthesis, a DNA fragment encoding the SARS-CoV-2 P2

280 S protein (based on GenBank: MN908947), including the amino acid exchanges K986P and

281 V987P, was cloned into a starting plasmid vector with backbone sequence elements for

282 improved RNA stability and translational efficiency[19,34]. Non-coding backbone elements

283 included the regions from the T7 promoter to the 5′ and 3′ UTR plus a poly(A) tail

284 (100 nucleotides) interrupted by a linker (A30LA70, 10 nucleotides). The DNA was purified,

285 spectrophotometrically quantified, and *in vitro* transcribed by T7 RNA polymerase in the

286 presence of a trinucleotide cap1 analogue $((m_2^{7,3'-O})Gppp(m^{2'-O})ApG$; TriLink) and of N^1-

287 methylpseudouridine-5'-triphosphate (m1ΨTP; Thermo Fisher Scientific) instead of uridine-

288 5'-triphosphate (UTP)[35]. RNA was purified using magnetic particles[36], integrity assessed by

289 microfluidic capillary electrophoresis (Agilent Fragment Analyser), and concentration, pH,

290 osmolality, endotoxin level and bioburden determined.

Lipid-nanoparticle formulation of the RNA.

Purified RNA was formulated into LNPs using an ethanolic lipid mixture of ionisable cationic lipid and transferred into an aqueous buffer system via diafiltration to yield an LNP composition similar to one previously described[37]. BNT162b2 was stored at -70 °C at a concentration of 0.5 mg/mL.

mRNA transfection and P2 S translation.

HEK293T/17 cells were transfected with 1 μg RiboJuice transfection reagent-mixed BNT162b2 RNA or with BNT162b2 (BNT162b2 RNA formulated as LNP) by incubation for 18 hours. Non-LNP formulated mRNA was diluted in Opti-MEM medium (Thermo Fisher Scientific) and mixed with the transfection reagents according to the manufacturer's instructions (RiboJuice, Merck Millipore). Transfected HEK293T/17 cells were stained with Fixable Viability Dye (eBioscience). After fixation (Fixation Buffer, BioLegend), cells were permeabilised (Perm Buffer, eBioscience) and stained with a monoclonal SARS-CoV-2 spike S1 antibody (SinoBiological). Cells were acquired on a FACSCanto II flow cytometer (BD Biosciences) using BD FACSDiva software version 8.0.1 and analysed by FlowJo software version 10.6.2 (FlowJo LLC, BD Biosciences).

P2 S expression and purification.

To express P2 S for structural characterisation, a gene encoding the full length of SARS-CoV-2 (GenBank: MN908947) with two prolines substituted at residues 986 and 987 followed with a C-terminal HRV3C protease site and a TwinStrep tag was cloned into a modified pcDNA3.1(+) vector with the CAG promoter. The TwinStrep-tagged P2 S was expressed in Expi293 cells. Purification of the recombinant protein was based on a procedure described previously, with minor modifications[5]. Upon cell lysis, P2 S was solubilized in 1% NP-40 detergent. The TwinStrep-tagged protein was then captured with StrepTactin Sepharose HP resin in 0.5% NP-40. P2 S was further purified by size-exclusion chromatography and eluted as three distinct peaks in 0.02 % NP-40 as previously reported[5]. Peak 1, which consists of intact P2 S migrating at around 150 kDa, as well as dissociated S1 and S2 subunits, which co-migrate at just above 75 kDa, was used in the structural characterisation. Spontaneous dissociation of the S1 and S2 subunits mostly occurs throughout the course of the protein purification, starting at the point of detergent-mediated protein extraction.

Biolayer interferometry.

322   The binding of detergent NP-40 solubilized, purified P2 S to human ACE2 peptidase domain

323   (ACE2 PD) and human neutralising monoclonal antibody B38[22] was performed on Octet

324   RED384 (FortéBio) at 25 °C in a running buffer (RB) consisting of 25 mM Tris pH7.5, 150 mM

325   NaCl, 1 mM EDTA and 0.02% NP-40. Avi-tagged ACE2-PD was captured on streptavidin

326   coated sensors and B38 antibody was captured on sensors coated with protein G. After initial

327   baseline equilibration of 120 s, the sensors were dipped in 10 µg/mL solution of Avi-tagged

328   ACE2-PD or B38 mAb for 300 s to achieve capture levels of 1 nM using the threshold function.

329   The sensors were dipped in RB for 120 s for collecting baseline before they were dipped in a

330   concentration series of purified P2 S samples for 300 s (association phase). The sensors were

331   immersed in RB for measuring 600 s (dissociation phase). Data were reference subtracted and

332   fit to a 1:1 binding model with R^2 value greater than 0.95, to determine kinetics and affinity of

333   binding, using Octet Data Analysis Software v10.0 (FortéBio).

Cryo-electron microscopy sample preparation, data collection and data processing.

335   For TwinStrep-tagged P2 S, 4 µL purified protein at 0.5 mg/mL were applied to gold Quantifoil

336   R1.2/1.3 300 mesh grids freshly overlaid with graphene oxide. Sample was blotted using a

337   Vitrobot Mark IV for 4 s with a force of -2 before being plunged into liquid ethane cooled by

338   liquid nitrogen. 27,701 micrographs were collected from a two identically prepared grids on a

339   Titan Krios operating at 300 keV equipped with a Gatan K2 Summit direct electron detector in

340   super-resolution mode at a magnification of 165,000x, for a magnified pixel size of 0.435 Å at

341   the specimen level. Data were collected from each grid over a defocus range of -1.2 to -3.4 µm

342   with a total electron dose of 50.32 and 50.12 e$^-$/Å^2, respectively, fractionated into 40 frames

343   over a 6-second exposure for 1.26 and 1.25 e$^-$/Å^2/frame. On-the-fly motion correction, CTF

344   estimation, and particle picking and extraction with a box size of 450 pixels were performed in

345   Warp[38], during which super-resolution data were binned to give a pixel size of 0.87 Å. A total

346   of 1,119,906 particles were extracted. All subsequent processing was performed in RELION

347   3.1-beta[39]. Particle heterogeneity was filtered out with 2D and 3D classification to filter out bad

348   particles, yielding a set of 73,393 particles, which refined to 3.6 Å with C3 symmetry. 3D

349   classification of this dataset without particle alignment separated out one class with a single

350   RBD up, representing 15,098 particles. The remaining 58,295 particles, in three RBD 'down'

351   conformation, were refined to give a final model at 3.29 Å. The atomic model from PDB ID

352   6XR8[5] was rigid-body fitted into the map density, then flexibly fitted to the density using real-

353   space refinement in Phenix[40] alternating with manual building in Coot[41]. The cryo-EM model

354   validation is provided in Extended Data Fig 3b, the full cryo-EM data processing workflow in

355   Extended Data Fig. 3c, and the model refinement statistics in Extended Data Table 1.

356   **Immunisation.**

357   *Mice.* Female BALB/c mice (Janvier; 8-12 weeks) and were randomly allocated to groups.

358   BNT162b2 was diluted in PBS, 300 mM sucrose or saline (0.9% NaCl) and injected IM into

359   the gastrocnemius muscle at a volume of 20 µL under isoflurane anaesthesia.

360   *Rhesus macaques* (*Macaca mulatta*). Male rhesus macaques (2–4 years) were randomly

361   assigned to receive either BNT162b2 or saline placebo control in 0.5 mL volume administered

362   by IM injection in the left quadriceps muscle on Days 0 and 21.

363   **Tissue preparation.**

364   *Mice.* Peripheral blood was collected from the retro-orbital venous plexus under isoflurane

365   anaesthesia or *vena facialis* without prior anesthetisation. Blood was centrifuged for 5 minutes

366   at 16.000 x g, and the serum was immediately used for downstream assays or stored at -20 °C.

367   Spleen single-cell suspensions were prepared in PBS by mashing tissue against the surface of

368   a 70 µm cell strainer (BD Falcon). Erythrocytes were removed by hypotonic lysis. Popliteal,

369   inguinal and iliac lymph nodes were pooled, cut into pieces, digested with collagenase D

370   (1 mg/mL; Roche) and passed through cell strainers.

371   *Rhesus macaques* (*Macaca mulatta*). Serum was obtained before immunisation and on Days

372   14, 21, 28, 35, 42, and 56. PBMCs were obtained before immunisation and on Days 7, 28, and

373   42, except that PBMCs were not obtained from the buffer-immunised group on Day 28. Blood

374   for serum and PBMCs was collected in compliance with animal protocol 2017-8725-023

375   approved by the NIRC Institutional Animal Care and Use Committee. Animals were

376   anesthetised with ketamine HCl (10 mg/kg; IM) during blood collection and immunisation, and

377   monitored for adequate sedation.

378   **S1- and RBD-binding IgG assay.**

379   For mouse sera, MaxiSorp plates (Thermo Fisher Scientific) were coated with recombinant S1

380   or RBD (100 ng/100 µL) in sodium carbonate buffer, and bound IgG was detected using an

381   HRP-conjugated secondary antibody and TMB substrate (Biotrend). Data collection was

382   performed using a BioTek Epoch reader and Gen5 software version 3.0.9. For concentration

383   analysis, the signal of the specific samples was correlated to a standard curve of an isotype

384 control. For rhesus macaque and human sera, a recombinant SARS-CoV-2 S1 containing a C-
385 terminal Avitag™ (Acro Biosystems) was bound to streptavidin-coated Luminex microspheres.
386 Bound rhesus macaque or human anti-S1 antibodies present in the serum were detected with a
387 fluorescently labelled goat anti-human polyclonal secondary antibody (Jackson
388 ImmunoResearch). Data were captured as median fluorescent intensities (MFIs) using a
389 Bioplex200 system (Bio-Rad) and converted to U/mL antibody concentrations using a reference
390 standard consisting of 5 pooled human COVID-19 convalescent serum samples (obtained >14
391 days PCR diagnosis), diluted in antibody depleted human serum with arbitrary assigned
392 concentrations of 100 U/mL and accounting for the serum dilution factor.

393 **Binding kinetics of antigen-specific IgGs using surface plasmon resonance spectroscopy**
394 Binding kinetics of murine S1- and RBD-specific serum IgGs was determined using a Biacore
395 T200 device (Cytiva) with HBS-EP running buffer (BR100669, Cytiva) at 25 °C. Carboxyl
396 groups on the CM5 sensor chip matrix were activated with a mixture of 1-ethyl-3-(3-
397 dimethylaminopropyl) carbodiimidehydrochloride (EDC) and N-hydroxysuccinimide (NHS) to
398 form active esters for the reaction with amine groups. Anti-mouse-Fc-antibody (Jackson
399 ImmunoResearch) was diluted in 10 mM sodium acetate buffer pH 5 (30 µg/mL) for covalent
400 coupling to immobilisation level of ~10,000 response units (RU). Free N-hydroxysuccinimide
401 esters on the sensor surface were deactivated with ethanolamine.

402 Mouse serum was diluted 1:50 in HBS-EP buffer and applied at 10 µL/min for 30 seconds to
403 the active flow cell for capture by immobilised antibody, while the reference flow cell was
404 treated with buffer. Binding analysis of captured murine IgG antibodies to S1-His or RBD-His
405 (Sino Biological) was performed using a multi-cycle kinetic method with concentrations
406 ranging from 25 to 400 nM or 1.5625 to 50 nM, respectively. An association period of 180
407 seconds was followed by a dissociation period of 600 seconds with a constant flow rate of 40
408 µL/min and a final regeneration step. Binding kinetics were calculated using a global kinetic fit
409 model (1:1 Langmuir, Biacore T200 Evaluation Software Version 3.1, Cytiva).

410 **VSV-SARS-CoV-2 spike variant pseudovirus neutralisation.**
411 A recombinant replication-deficient vesicular stomatitis virus (VSV) vector that encodes GFP
412 instead of VSV-G (VSVΔG-GFP) was pseudotyped with SARS-CoV-2 S protein according to
413 published pseudotyping protocols[42,43]. In brief, HEK293T/17 monolayers transfected to express
414 SARS-CoV-2 S truncated of the C-terminal cytoplasmic 19 amino acids (SARS-CoV-2-S-

Page 14

415   CΔ19) were inoculated with VSVΔG-GFP vector. After incubation for 1 hour at 37 °C, the

416   inoculum was removed and cells were washed with PBS before medium supplemented with

417   anti-VSV-G antibody (clone 8G5F11, Kerafast Inc.) was added to neutralise residual input

418   virus. VSV/SARS-CoV-2 pseudovirus-containing medium was harvested 20 hours after

419   inoculation, 0.2 µm filtered and stored at -80 °C.

420   Serial dilutions of mouse serum samples were prepared and pre-incubated for 10 minutes at

421   room temperature with VSV/SARS-CoV-2 pseudovirus suspension (4.8×10^3 infectious units

422   [IU]/mL) before transferring the mix to Vero 76 cells. Inoculated Vero-76 cells were incubated

423   for 20 hours at 37 °C. Plates were placed in an IncuCyte Live Cell Analysis system (Sartorius)

424   and incubated for 30 minutes prior to the analysis (IncuCyte 2019B Rev2 software). Whole

425   well scanning for brightfield and GFP fluorescence was performed using a 4× objective. The

426   50% pseudovirus neutralisation titre ($pVNT_{50}$) was reported as the reciprocal of the first serum

427   dilution yielding a 50% reduction in GFP-positive infected cell number per well compared to

428   the mean of the no serum pseudovirus positive control. Each serum sample dilution was tested

429   in duplicates.

430   **IFNγ and IL-4 ELISpot.**

431   Murine ELISpot assays were performed with mouse IFNγ ELISpot[PLUS] kits according to the

432   manufacturer's instructions (Mabtech). A total of 5×10^5 splenocytes was *ex vivo* restimulated

433   with the full-length S peptide mix (0.1 µg/mL final concentration per peptide) or controls

434   (gp70-AH1 [SPSYVYHQF][33], 4 µg/mL; Concanavalin A [ConA], 2 µg/mL [Sigma]).

435   Streptavidin-alkaline phosphatase (ALP) and BCIP/NBT-plus substrate were added, and spots

436   counted using an ELISpot plate reader (ImmunoSpot® S6 Core Analyzer [CTL]). Spot numbers

437   were evaluated using ImmunoCapture Image Aquision Software V7.0 and ImmunoSpot

438   7.0.17.0 Professional. Spot counts denoted too numerous to count by the software were set to

439   1,500. For T-cell subtyping, CD8^{+} T cells and CD4^{+} T cells were isolated from splenocyte

440   suspensions using MACS MicroBeads (CD8a [Ly-2] and CD4 [L3T4] [Miltenyi Biotec])

441   according to the manufacturer's instructions. 1×10^5 CD8^{+} or CD4^{+} T cells were subsequently

442   restimulated with 5×10^4 syngeneic bone marrow-derived dendritic cells loaded with full-

443   length S peptide mix (0.1 µg/mL final concentration per peptide) or cell culture medium as

444   control. Purity of isolated T-cell subsets was determined by flow cytometry.

445   Rhesus macaque PBMCs were tested with commercially available NHP IFNγ and IL-4 ELISpot

446   assay kits (Mabtech, Sweden). Cryopreserved rhesus macaque PBMCs were thawed in pre-

447 warmed AIM-V media (Thermo Fisher Scientific, US) with Benzonase (EMD Millipore, US).

448 For IFNγ ELISpot, 1.0×10^5 PBMCs and 2.5×10^5 PBMCs for IL-4 ELISpot were stimulated

449 *ex vivo* with 1 µg/mL of the full-length S overlapping peptide mix. Tests were performed in

450 triplicate wells and media-DMSO, a CMV peptide pool and PHA (Sigma) were included as

451 controls. After 24 hours for IFNγ and 48 hours for IL-4, Streptavidin-HRP and AEC substrate

452 (BD Bioscience) were added, and spots counted using a CTL ImmunoSpot S6 Universal

453 Analyzer (CTL, US). Results shown are background (Media-DMSO) subtracted and

454 normalized to SFC/10^6 PBMCs.

Flow cytometry for analysis of cell mediated immunity.

456 For mouse T-cell analysis in peripheral blood, erythrocytes from 50 µL freshly drawn blood

457 were lysed (ACK lysing buffer [Gibco]), and cells were stained with Fixable Viability Dye

458 (eBioscience) and primary antibodies in the presence of Fc block in flow buffer (DPBS [Gibco]

459 supplemented with 2% FCS, 2 mM EDTA [both Sigma] and 0.01% sodium azide [Morphisto]).

460 After staining with secondary biotin-coupled antibodies in flow buffer, cells were stained

461 extracellularly against surface markers with directly labelled antibodies and streptavidin in

462 Brilliant Stain Buffer Plus (BD Bioscience) diluted in flow buffer. Cells were washed with 2%

463 RotiHistofix (Carl Roth), fixed (Fix/Perm Buffer, FoxP3/Transcription Factor Staining Buffer

464 Set [eBioscience]) and permeabilised (Perm Buffer, FoxP3/Transcription Factor Staining

465 Buffer Set [eBioscience]) overnight. Permeabilised cells were intracellularly treated with Fc

466 block and stained with antibodies against transcription factors in Perm Buffer.

467 For mouse T-cell analysis in lymphoid tissues, 1.5×10^6 lymph node and 4×10^6 spleen cells

468 were stained for viability and extracellular antigens with directly labelled antibodies. Fixation,

469 permeabilisation and intracellular staining was performed as described for blood T-cell staining.

470 For mouse B-cell subtyping in lymphoid tissues, 2.5×10^5 lymph node and 1×10^6 spleen cells

471 were treated with Fc block, stained for viability and extracellular antigens as described for blood

472 T-cell staining and fixed with 2% RotiHistofix overnight.

473 For mouse intracellular cytokine staining in T cells, 4×10^6 spleen cells were *ex vivo*

474 restimulated with 0.5 µg/mL final concentration per peptide of full-length S peptide mix or cell

475 culture medium (no peptide) as control in the presence of GolgiStop and GolgiPlug (both BD

476 Bioscience) for 5 hours. Cells were stained for viability and extracellular antigens as described

477   for lymphoid T-cell staining. Cells were fixed with 2% RotiHistofix and permeabilised

478   overnight. Intracellular staining was performed as described for blood T-cell staining.

479   Mouse cells were acquired on a BD Symphony A3 or BD Celesta (B-cell subtyping) flow

480   cytometer (BD Bioscience) using BD FACSDiva software version 9.1 or 8.0.1.1, respectively,

481   and analysed with FlowJo 10.6 (FlowJo LLC, BD Biosciences).

482   For rhesus macaques intracellular cytokine staining in T cells, 1.5×10^6 PBMCs were stimulated

483   with the full-length S peptide mix at 1 µg/mL, Staphyloccocus enterotoxin B (SEB; 2 µg/mL)

484   as positive control, or 0.2% DMSO as negative control. GolgiStop and GolgiPlug (both BD

485   Bioscience) were added. Following 37 °C incubation for 12 to 16 h, cells were stained for

486   viability and extracellular antigens after blocking Fc binding sites with directly labelled

487   antibodies. Cells were then fixed and permeabilized with BDCytoFix/CytoPerm solution (BD

488   Bioscience), intracellular staining was performed in perm buffer for 30 min at RT. Cells were

489   washed, resuspended in 2% FBS/PBS buffer and acquired on a LSR Fortessa. Data analyzed

490   by FlowJo (10.4.1). Results shown are background (Media-DMSO) subtracted.

491   **Cytokine profiling.**

492   Mouse splenocytes were re-stimulated for 48 hours with full-length S peptide mix (0.1 µg/mL

493   final concentration per peptide) or cell culture medium (no peptide) as control. Concentrations

494   of IFNγ, IL-2, IL-4, IL-5 and IL-13 in supernatants were determined using a bead-based, 11-

495   plex T_H1/T_H2 mouse ProcartaPlex multiplex immunoassay (Thermo Fisher Scientific)

496   according to the manufacturer's instructions. Fluorescence was measured with a Bioplex200

497   system (Bio-Rad) and analysed with ProcartaPlex Analyst 1.0 software (Thermo Fisher

498   Scientific). Values below the lower limit of quantification (LLOQ) were set to zero.

499   **SARS-CoV-2 neutralisation.**

500   The SARS-CoV-2 neutralisation assay used a previously described strain of SARS-CoV-2

501   (USA_WA1/2020) that had been rescued by reverse genetics and engineered by the insertion

502   of an mNeonGreen (mNG) gene into open reading frame 7 of the viral genome[25]. This reporter

503   virus generates similar plaque morphologies and indistinguishable growth curves from wild-

504   type virus. Viral master stocks were grown in Vero 76 cells as previously described[44]. When

505   testing human convalescent serum specimens, the fluorescent neutralisation assay produced

506   comparable results as the conventional plaque reduction neutralisation assay. Serial dilutions

507 of heat-inactivated sera were incubated with the reporter virus (2 x 10^4 PFU per well) to yield

508 approximately a 10-30% infection rate of the Vero CCL81 monolayer for 1 hour at 37 °C before

509 inoculating Vero CCL81 cell monolayers (targeted to have 8,000 to 15,000 cells in the central

510 field of each well at the time of seeding, one day before infection) in 96-well plates to allow

511 accurate quantification of infected cells. Cell counts were enumerated by nuclear stain (Hoechst

512 33342) and fluorescent virally infected foci were detected 16-24 hours after inoculation with a

513 Cytation 7 Cell Imaging Multi-Mode Reader (Biotek) with Gen5 Image Prime version 3.09.

514 Titers were calculated in GraphPad Prism version 8.4.2 by generating a 4- parameter (4PL)

515 logistical fit of the percent neutralisation at each serial serum dilution. The 50% neutralisation

516 titre (VNT_{50}) was reported as the interpolated reciprocal of the dilution yielding a 50%

517 reduction in fluorescent viral foci.

518 **SARS-CoV-2 challenge of rhesus macaques (*Macaca mulatta*).**

519 The SARS-CoV-2 inoculum was obtained from a stock of 2.1×10^6 PFU/mL previously

520 prepared at Texas Biomedical Research Institute (San Antonio, TX), aliquoted into single use

521 vials, and stored at -70 °C. The working virus stock was generated from two passages of the

522 SARS-CoV-2 USA-WA1/2020 isolate (a 4th passage seed stock purchased from BEI Resources;

523 NR-52281) in Vero 76 cells. The virus was confirmed to be SARS-CoV-2 by deep sequencing

524 and identical to the published sequence (GenBank accession number MN985325.1).

525 BNT162b2-immunised (n=6) and age-matched saline control-immunised (n=3) male rhesus

526 macaques (control) were challenged with 1.05×10^6 plaque forming units of SARS-CoV-2

527 USA-WA1/2020 isolate, split equally between the intranasal (IN; 0.25 mL) and intratracheal

528 (IT; 0.25 mL) routes as previously described[26]. The challenge was performed 55 days after the

529 second immunisation. A separate sentinel group of non-immunised age- and sex-matched

530 animals (n=3) was mock challenged with DMEM supplemented with 10% FCS IN (0.25 mL)

531 and IT (0.25 mL). Approximately two weeks prior to challenge, animals were moved to the

532 ABSL-3 facility at Southwest National Primate Research Center (SNPRC; San Antonio, TX).

533 Animals were monitored regularly by a board-certified veterinary clinician for rectal body

534 temperature, weight and physical examination. Specimen collection was performed under

535 tiletamine zolazepam (Telazol) anaesthesia as described[26]. Nasal and oropharyngeal swabs

536 were collected from all macaques at Day 0, 1, 3, and 6 (relative to the day of challenge), from

537 BNT162b2-immunised macaques on Day 7 or 8, and from control and sentinel macaques on

538   Day 10. Bronchoalveolar lavage (BAL) was performed on all macaques the week before

539   challenge and on Days 3 and 6 post-challenge and on BNT162b2-immunised macaques on Day

540   7 or 8. BAL was performed by instilling four times 20 mL of saline. These washings were

541   pooled, aliquoted and stored frozen at -70 °C. Necropsy was performed on BNT162b2-

542   immunised animals on Day 7 or 8. Control and sentinel animals were not necropsied to allow

543   re-challenge (control) or challenge (sentinel) on a subsequent day.

544   **Reverse-transcription quantitative polymerase chain reaction.**

545   To detect and quantify SARS-CoV-2 in NHP, viral RNA was extracted from nasal swabs, OP

546   swabs, and BAL specimens as previously described[45–47] and tested by RT-qPCR as previously

547   described[26]. Briefly, 10 µg yeast tRNA and 1×10^3 PFU of MS2 phage (*Escherichia coli*

548   bacteriophage MS2, ATCC) were added to each thawed sample, and RNA extraction performed

549   using the NucleoMag Pathogen kit (Macherey-Nagel). The SARS-CoV-2 RT-qPCR was

550   performed on extracted RNA using a CDC-developed 2019-nCoV_N1 assay on a QuantStudio

551   3 instrument (Applied Biosystems). The cut-off for positivity (limit of detection, LOD) was

552   established at 10 gene equivalents (GE) per reaction (800 GE/mL). Samples were tested in

553   duplicate. On day 6, one BAL specimen from the control group and one day 1 nasal swab from

554   the BNT162b1-immunised group had, on repeated measurements, viral RNA levels on either

555   side of the LLOD. These specimens were categorised as indeterminate and excluded from the

556   graphs and the analysis.

557   **Statistics and reproducibility.**

558   No statistical methods were used to predetermine group and samples sizes (n). All experiments

559   were performed once. P-values reported for RT-qPCR analysis were determined by

560   nonparametric analysis (Friedman's test) based on the ranking of viral RNA shedding data

561   within each day. PROC RANK and PROC GLM from SAS® 9.4 were used to calculate the p-

562   values. Samples from post challenge days (Days 3, 6 and end of protocol [EOP] for BAL; Days

563   1, 3, 6 and 10 [control and sentinel] or EOP [BNT162b2-immunised] for nasal and

564   oropharyngeal swabs) were included in the analysis. Indeterminate results were excluded from

565   this analysis. All remaining analyses were carried out using GraphPad Prism 8.4.

Data availability.

The data that support the findings of this study are available from the corresponding author upon reasonable request.

Acknowledgements

Author Contributions

U.S. conceived and conceptualised the work and strategy. S.He., S.C.D., C.K. and M.C.G. designed primers and cloned all constructs. T.Z., S.F., J.S. and A.N.K. developed, planned, performed and supervised RNA synthesis and analysis. E.H.M. purified P2 S. P.V.S. developed and performed biolayer interferometry. J.A.L. and S.H. performed electron microscopy and solved the structure of the complex. Y.C. supervised the structural and biophysical characterisation and analysed the structures. A.M. and B.G.L. performed surface plasmon resonance spectroscopy. A.G. and S.A.K. planned, performed and analysed *in vitro* studies. F.B., T.K., C.R. managed formulation strategy. A.B.V., M.V., L.M.K. designed mouse studies and analysed and interpreted data. A.P., S.E., D.P. and G.S. performed and analysed the S1-binding IgG assays. R.C., Jr. and K.J.A. performed and analysed viral RT-qPCR data. A.M.,

595   B.S., A.W., C.F.-G. and P.-Y.S. performed and analysed pVNT and VNT assays. D.E., D.S.,

596   B.J., Y.F, H.J. performed *in vivo* studies and ELISpot assays. A.B.V., K.C.W. J.L., M.S.M. and

597   M.V. planned, analysed and interpreted ELISpot assays. L.M.K., J.L., D.E., Y.F., H.J., A.P.H.

598   M.S.M. and P.A planned, performed and analysed flow cytometry assays. A.B.V., L.M.K., Y.F.

599   and H.J. planned, performed, analysed and interpreted cytokine release assays. I.K., K.A.S.,

600   K.T., D.K. and P.R.D. designed NHP studies and analysed and interpreted data. K.T., M.P.,

601   I.L.S. and W.K. oversaw NHP immunogenicity and serology testing. S.H.-U. and K.B. provided

602   veterinary services for NHPs. J.C., T.C. and J.O managed the NHP colony. A.B.V., I.K., Y.C.,

603   A.M., M.V, L.M.K., C.T., K.S., Ö.T., P.R.D, K.U.J. and U.S. wrote the manuscript. All authors

604   supported the review of the manuscript.

Competing interests

606   The authors declare: U.S. and Ö.T. are management board members and employees at

607   BioNTech SE (Mainz, Germany); K.C.W., B.G.L., D.S., B.J., T.K. and C.R. are employees at

608   BioNTech SE; A.B.V., A.M., M.V., L.M.K., S.He., A.G., T.Z., A.P., D.E., S.C.D., S.F., S.E.,

609   F.B., B.S., A.W., Y.F., H.J., S.A.K., A.P.H., P.A., J.S., C.K., and A.N.K. are employees at

610   BioNTech RNA Pharmaceuticals GmbH (Mainz, Germany); A.B.V., A.M., K.C.W., A.G., S.F.,

611   A.N.K and U.S. are inventors on patents and patent applications related to RNA technology and

612   COVID-19 vaccine; A.B.V., A.M., M.V., L.M.K., K.C.W., S.He., B.G.L., A.P., D.E., S.C.D.,

613   S.F., S.E., D.S., B.J., B.S., A.P.H., P.A., J.S., C.K., T.K., C.R., A.N.K., Ö.T. and U.S. have

614   securities from BioNTech SE; I.K., Y.C., K.A.S., J.L., M.M., K.T., M.C.G., S.H.,

615   J.A.L.,E.H.M., P.V.S., C.Y.T., D.P., G.S., M.P., I.L.S., T.C., J.O., W.V.K., P.R.D. and K.U.J.

616   are employees of Pfizer and may hold stock options;

617   C.F.-G. and P.-Y.S. received compensation from Pfizer to perform neutralisation assays;

618   J.C., S.H.-U, K.B., R.C., jr., K.J.A. and D.K., are employees of Southwest National Primate

619   Research Center, which received compensation from Pfizer to conduct the animal challenge

620   work;

621   no other relationships or activities that could appear to have influenced the submitted work.

Funding

Additional Information

Supplementary Information is available for this study.

Correspondence and requests for materials should be addressed to Ugur Sahin.

References

1. Zhu, N. *et al.* A Novel Coronavirus from Patients with Pneumonia in China, 2019. *The New England journal of medicine* **382,** 727−733; 10.1056/NEJMoa2001017 (2020).

2. Zhou, P. *et al.* A pneumonia outbreak associated with a new coronavirus of probable bat origin. *Nature* **579,** 270−273; 10.1038/s41586-020-2012-7 (2020).

3. Yan, R. *et al.* Structural basis for the recognition of SARS-CoV-2 by full-length human ACE2. *Science (New York, N.Y.)* **367,** 1444−1448; 10.1126/science.abb2762 (2020).

4. Yi, C. *et al.* Key residues of the receptor binding motif in the spike protein of SARS-CoV-2 that interact with ACE2 and neutralizing antibodies. *Cellular & molecular immunology*; 10.1038/s41423-020-0458-z (2020).

5. Cai, Y. *et al.* Distinct conformational states of SARS-CoV-2 spike protein. *Science (New York, N.Y.)*; 10.1126/science.abd4251 (2020).

6. Ou, X. *et al.* Characterization of spike glycoprotein of SARS-CoV-2 on virus entry and its immune cross-reactivity with SARS-CoV. *Nature communications* **11,** 1620; 10.1038/s41467-020-15562-9 (2020).

7. Fan, X., Cao, D., Kong, L. & Zhang, X. Cryo-EM analysis of the post-fusion structure of the SARS-CoV spike glycoprotein. *Nature communications* **11,** 3618; 10.1038/s41467-020-17371-6 (2020).

8. Kirchdoerfer, R. N. *et al.* Stabilized coronavirus spikes are resistant to conformational changes induced by receptor recognition or proteolysis. *Scientific reports* **8,** 15701; 10.1038/s41598-018-34171-7 (2018).

9. Pallesen, J. *et al.* Immunogenicity and structures of a rationally designed prefusion MERS-CoV spike antigen. *Proceedings of the National Academy of Sciences of the United States of America* **114,** E7348-E7357; 10.1073/pnas.1707304114 (2017).

10. Wrapp, D. *et al.* Cryo-EM structure of the 2019-nCoV spike in the prefusion conformation. *Science (New York, N.Y.)* **367,** 1260−1263; 10.1126/science.abb2507 (2020).

659   11. Brouwer, P. J. M. *et al.* Potent neutralizing antibodies from COVID-19 patients define
660   multiple targets of vulnerability. *Science (New York, N.Y.)*; 10.1126/science.abc5902
661   (2020).

662   12. Chi, X. *et al.* A neutralizing human antibody binds to the N-terminal domain of the Spike
663   protein of SARS-CoV-2. *Science (New York, N.Y.)*; 10.1126/science.abc6952 (2020).

664   13. Jackson, L. A. *et al.* An mRNA Vaccine against SARS-CoV-2 - Preliminary Report. *The*
665   *New England journal of medicine*; 10.1056/NEJMoa2022483 (2020).

666   14. Zhu, F.-C. *et al.* Safety, tolerability, and immunogenicity of a recombinant adenovirus type-
667   5 vectored COVID-19 vaccine. A dose-escalation, open-label, non-randomised, first-in-
668   human trial. *The Lancet* **395,** 1845−1854; 10.1016/S0140-6736(20)31208-3 (2020).

669   15. Walsh, E. E. *et al.* RNA-Based COVID-19 Vaccine BNT162b2 Selected for a Pivotal
670   Efficacy Study. *medRxiv 2020*; 10.1101/2020.08.17.20176651 (2020).

671   16. Folegatti, P. M. *et al.* Safety and immunogenicity of the ChAdOx1 nCoV-19 vaccine against
672   SARS-CoV-2. A preliminary report of a phase 1/2, single-blind, randomised controlled trial.
673   *The Lancet* **396,** 467−478; 10.1016/S0140-6736(20)31604-4 (2020).

674   17. Pardi, N. *et al.* Expression kinetics of nucleoside-modified mRNA delivered in lipid
675   nanoparticles to mice by various routes. *Journal of controlled release : official journal of*
676   *the Controlled Release Society* **217,** 345−351; 10.1016/j.jconrel.2015.08.007 (2015).

677   18. Karikó, K. *et al.* Incorporation of pseudouridine into mRNA yields superior
678   nonimmunogenic vector with increased translational capacity and biological stability.
679   *Molecular therapy : the journal of the American Society of Gene Therapy* **16,** 1833−1840;
680   10.1038/mt.2008.200 (2008).

681   19. Orlandini von Niessen, A. G. *et al.* Improving mRNA-Based Therapeutic Gene Delivery by
682   Expression-Augmenting 3' UTRs Identified by Cellular Library Screening. *Mol Ther* **27,**
683   824−836; 10.1016/j.ymthe.2018.12.011 (2019).

684   20. Pardi, N. *et al.* Zika virus protection by a single low-dose nucleoside-modified mRNA
685   vaccination. *Nature* **543,** 248−251; 10.1038/nature21428 (2017).

686   21. Pardi, N. *et al.* Characterization of HIV-1 Nucleoside-Modified mRNA Vaccines in Rabbits
687   and Rhesus Macaques. *Molecular therapy. Nucleic acids* **15,** 36–47;
688   10.1016/j.omtn.2019.03.003 (2019).

689   22. Wu, Y. *et al.* A noncompeting pair of human neutralizing antibodies block COVID-19 virus
690   binding to its receptor ACE2. *Science (New York, N.Y.)* **368,** 1274–1278;
691   10.1126/science.abc2241 (2020).

692   23. Henderson, R. *et al.* Controlling the SARS-CoV-2 spike glycoprotein conformation. *Nature*
693   *structural & molecular biology*; 10.1038/s41594-020-0479-4 (2020).

694   24. Hutloff, A. Regulation of T follicular helper cells by ICOS. *Oncotarget* **6,** 21785–21786;
695   10.18632/oncotarget.4798 (2015).

696   25. Muruato, A. E. *et al.* A high-throughput neutralizing antibody assay for COVID-19
697   diagnosis and vaccine evaluation. *Nature communications* **11,** 4059; 10.1038/s41467-020-
698   17892-0 (2020).

699   26. Singh, D. K. *et al.* SARS-CoV-2 infection leads to acute infection with dynamic cellular
700   and inflammatory flux in the lung that varies across nonhuman primate species. *bioRxiv*
701   *2020.06.05.136481*; 10.1101/2020.06.05.136481 (2020).

702   27. Zost, S. J. *et al.* Rapid isolation and profiling of a diverse panel of human monoclonal
703   antibodies targeting the SARS-CoV-2 spike protein. *Nature medicine*; 10.1038/s41591-
704   020-0998-x (2020).

705   28. Yang, D. *et al.* Attenuated interferon and pro-inflammatory response in SARS-CoV-2-
706   infected human dendritic cells is associated with viral antagonism of STAT1
707   phosphorylation. *The Journal of infectious diseases*; 10.1093/infdis/jiaa356 (2020).

708   29. Jafarzadeh, A., Chauhan, P., Saha, B., Jafarzadeh, S. & Nemati, M. Contribution of
709   monocytes and macrophages to the local tissue inflammation and cytokine storm in COVID-
710   19: Lessons from SARS and MERS, and potential therapeutic interventions. *Life sciences,*
711   118102; 10.1016/j.lfs.2020.118102 (2020).

712   30. Lambert, P.-H. *et al.* Consensus summary report for CEPI/BC March 12-13, 2020 meeting:

713   Assessment of risk of disease enhancement with COVID-19 vaccines. *Vaccine* **38,** 4783–

714   4791; 10.1016/j.vaccine.2020.05.064 (2020).

715   31. Sahin, U. *et al.* Concurrent human antibody and T H 1 type T-cell responses elicited by a

716   COVID-19 RNA vaccine. *medRxiv 2020.07.17.20140533*; 10.1101/2020.07.17.20140533

717   (2020).

718   32. Mulligan, M. J. *et al.* Phase 1/2 study of COVID-19 RNA vaccine BNT162b1 in adults.

719   *Nature*; 10.1038/s41586-020-2639-4 (2020).

720   33. Slansky, J. E. *et al.* Enhanced antigen-specific antitumor immunity with altered peptide

721   ligands that stabilize the MHC-peptide-TCR complex. *Immunity* **13,** 529–538;

722   10.1016/S1074-7613(00)00052-2 (2000).

723   34. Holtkamp, S. *et al.* Modification of antigen-encoding RNA increases stability, translational

724   efficacy, and T-cell stimulatory capacity of dendritic cells. *Blood* **108,** 4009–4017;

725   10.1182/blood-2006-04-015024 (2006).

726   35. Grudzien-Nogalska, E. *et al.* Synthetic mRNAs with superior translation and stability

727   properties. *Methods in molecular biology (Clifton, N.J.)* **969,** 55–72; 10.1007/978-1-62703-

728   260-5_4 (2013).

729   36. Berensmeier, S. Magnetic particles for the separation and purification of nucleic acids.

730   *Appl.Microbiol.Biotechnol.* **73,** 495–504; 10.1007/s00253-006-0675-0 (2006).

731   37. Maier, M. A. *et al.* Biodegradable lipids enabling rapidly eliminated lipid nanoparticles for

732   systemic delivery of RNAi therapeutics. *Molecular therapy : the journal of the American*

733   *Society of Gene Therapy* **21,** 1570–1578; 10.1038/mt.2013.124 (2013).

734   38. Tegunov, D. & Cramer, P. Real-time cryo-electron microscopy data preprocessing with

735   Warp. *Nature methods* **16,** 1146–1152; 10.1038/s41592-019-0580-y (2019).

736   39. Zivanov, J. *et al.* New tools for automated high-resolution cryo-EM structure determination

737   in RELION-3. *eLife* **7**; 10.7554/eLife.42166 (2018).

738   40. Adams, P. D. *et al.* PHENIX: a comprehensive Python-based system for macromolecular

739   structure solution. *Acta crystallographica. Section D, Biological crystallography* **66,** 213–

740   221; 10.1107/S0907444909052925 (2010).

741   41. Emsley, P., Lohkamp, B., Scott, W. G. & Cowtan, K. Features and development of Coot.

742   *Acta crystallographica. Section D, Biological crystallography* **66,** 486–501;

743   10.1107/S0907444910007493 (2010).

744   42. Lester, S. *et al.* Middle East respiratory coronavirus (MERS-CoV) spike (S) protein

745   vesicular stomatitis virus pseudoparticle neutralization assays offer a reliable alternative to

746   the conventional neutralization assay in human seroepidemiological studies. *Access*

747   *Microbiology* **1,** 20290; 10.1099/acmi.0.000057 (2019).

748   43. Berger Rentsch, M. & Zimmer, G. A vesicular stomatitis virus replicon-based bioassay for

749   the rapid and sensitive determination of multi-species type I interferon. *PLoS ONE* **6,**

750   e25858; 10.1371/journal.pone.0025858 (2011).

751   44. Xie, X. *et al.* An Infectious cDNA Clone of SARS-CoV-2. *Cell host & microbe* **27,** 841-

752   848.e3; 10.1016/j.chom.2020.04.004 (2020).

753   45. Gautam, U. S. *et al.* In vivo inhibition of tryptophan catabolism reorganizes the tuberculoma

754   and augments immune-mediated control of Mycobacterium tuberculosis. *Proceedings of the*

755   *National Academy of Sciences of the United States of America* **115,** E62-E71;

756   10.1073/pnas.1711373114 (2018).

757   46. Mehra, S. *et al.* Granuloma correlates of protection against tuberculosis and mechanisms of

758   immune modulation by Mycobacterium tuberculosis. *The Journal of infectious diseases*

759   **207,** 1115–1127; 10.1093/infdis/jis778 (2013).

760   47. Joosten, S. A. *et al.* Mycobacterium tuberculosis peptides presented by HLA-E molecules

761   are targets for human CD8 T-cells with cytotoxic as well as regulatory activity. *PLoS*

762   *pathogens* **6,** e1000782; 10.1371/journal.ppat.1000782 (2010).
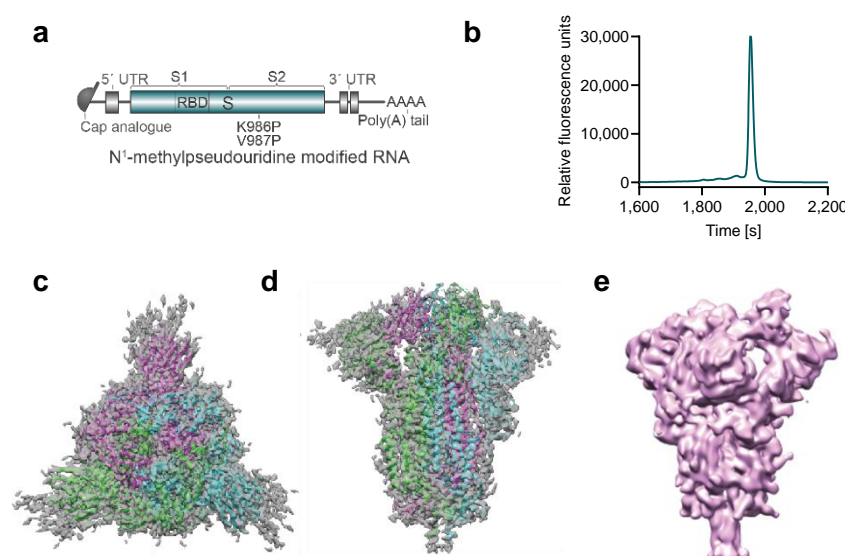
Figure 1. Vaccine design and characterisation of the expressed antigen.

a, BNT162b2 RNA structure. UTR, untranslated region; S, SARS-CoV-2 S glycoprotein; S1, N-terminal furin cleavage fragment; S2, C-terminal furin cleavage fragment; RBD, receptor-binding domain. Positions of the P2 mutation (K986P and V897P) are indicated. **b**, Liquid capillary electropherogram of *in vitro* transcribed BNT162b2 RNA. **c**, A 3.29 Å cryoEM map of P2 S, with fitted and refined atomic model, viewed down the three-fold axis toward the membrane. **d,** Cryo-EM map and model of (d) viewed perpendicular to the three-fold axis. **e,** Mass density map of TwinStrep-tagged P2 S produced by 3D classification of images extracted from cryo-EM micrographs with no symmetry averaging. This class, in the one-RBD 'up', two RBD 'down' positioning, represents 20.4% of the population.
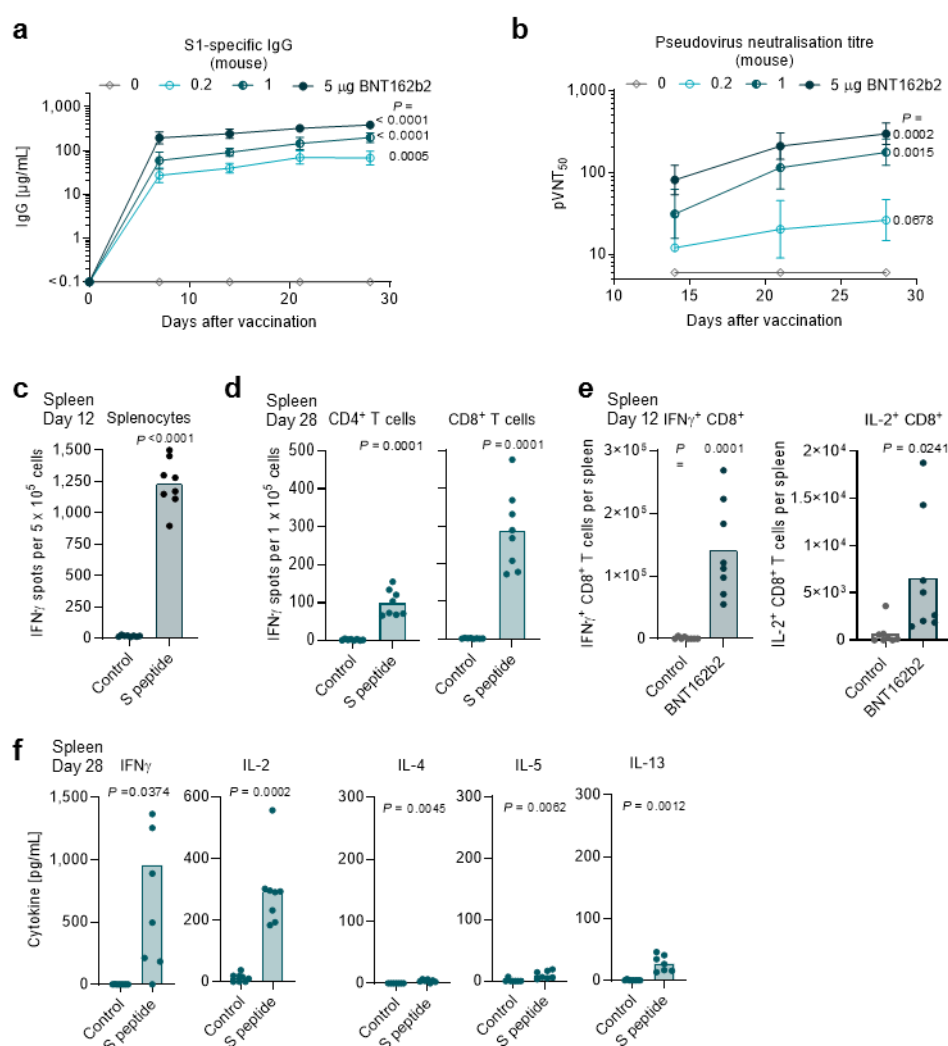
Figure 2. Mouse immunogenicity.

BALB/c mice (n=8 per group unless otherwise specified) were immunised intramuscularly (IM) with a single dose of with 0.2, 1 or 5 μg BNT162b2 or buffer. Geometric mean of each group ± 95% CI, P-values compare Day 28 to non-immunised (0 μg; n=8) baseline sera (multiple comparison of mixed-effect analysis using Dunnett's multiple comparisons test) (a, b). **a**, S1-binding IgG responses in sera obtained 7, 14, 21 and 28 days after immunisation with 0, 0.2, 1, or 5 μg BNT162b2, determined by ELISA. For day 0 values, a pre-screening of randomly selected animals was performed (n=4). **b,** VSV-SARS-CoV-2 pseudovirus 50% serum neutralising titers (pVNT$_{50}$) of sera from (a). **c-f,** Splenocytes of BALB/c mice immunised IM with BNT162b2 or buffer (control) were *ex vivo* re-stimulated with full-length S peptide mix or negative controls ([c], [e], [f]: no peptide; [d]: irrelevant peptide). Individual values and mean of each group, P-values were determined by a two-tailed paired t-test. **c**, IFNγ ELISpot of splenocytes collected 12 days after immunisation with 5 μg BNT162b2. **d**, IFNγ ELISpot of isolated splenic CD4$^+$ or CD8$^+$ T cells collected

28 days after immunisation with 1 µg BNT162b2. **e**, CD8^{+} T-cell specific cytokine release by splenocytes collected 12 days after immunisation with 5 µg BNT162b2 or buffer (Control), determined by flow cytometry. S-peptide specific responses are corrected for background (no peptide). **f**, Cytokine production by splenocytes collected 28 days after immunisation with 1 µg BNT162b2, determined by bead-based multiplex analysis (n=7 for IL-4, IL-5 and IL-13, one outlier removed via routs test [Q=1%] for the S peptide stimulated samples).
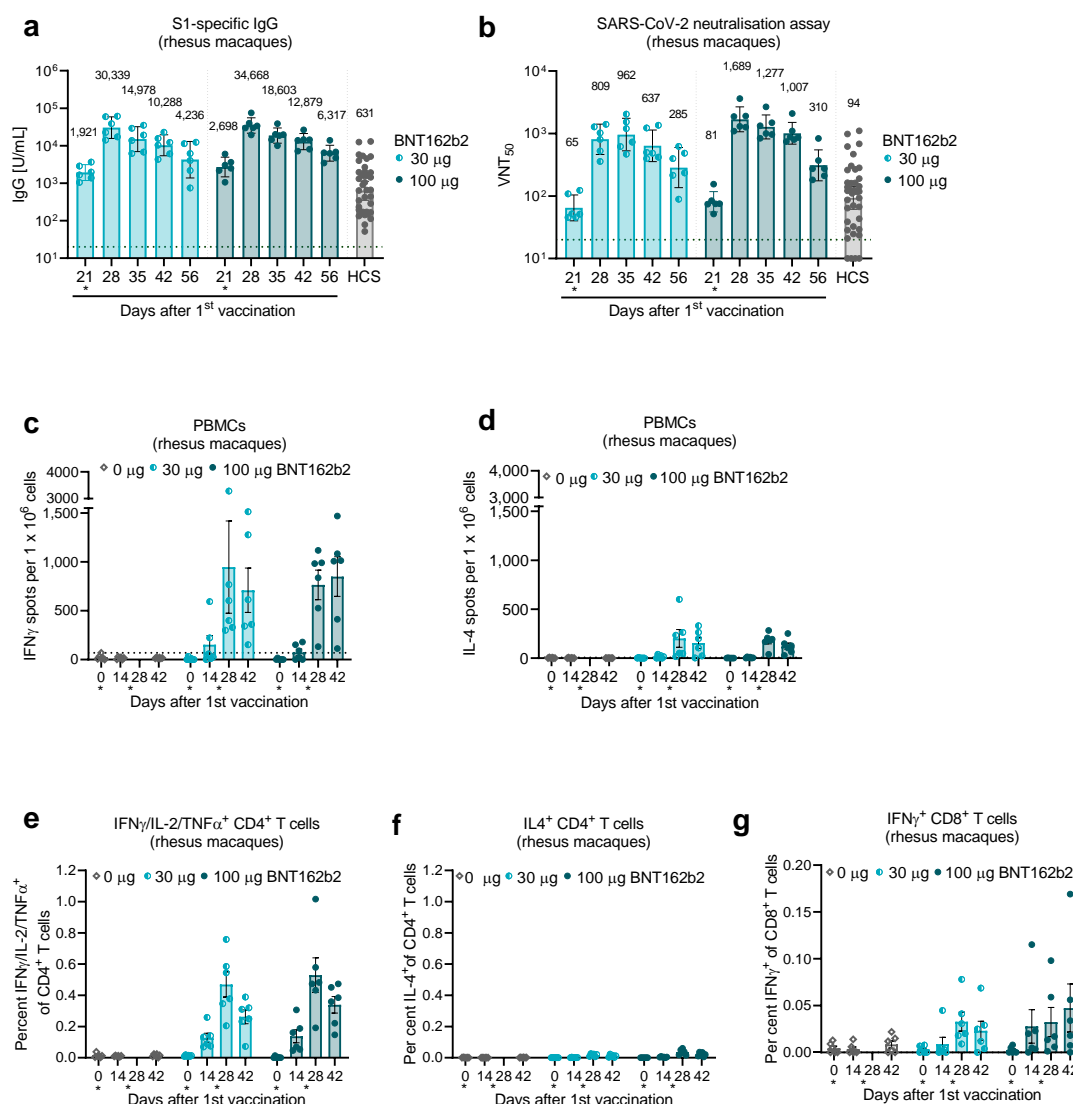
Figure 3. Rhesus macaque immunogenicity.

Rhesus macaques (n=6 per group) were immunised on Days 0 and 21 with 30 µg or 100 µg BNT162b2 or buffer. Sera and PBMCs were collected at the times indicated. Human convalescent sera (HCS) were obtained from SARS-CoV-2-infected patients at least 14 days after PCR-confirmed diagnosis and at a time when acute COVID-19 symptoms had resolved (n=38). **a**, Concentration, in arbitrary units, of IgG binding recombinant SARS-CoV-2 S1. **b**, SARS-CoV-2 50% virus neutralisation titers (VNT_{50}). **c-g**, PBMCs collected on Day 42 were *ex vivo* re-stimulated with full-length S peptide mix. **c**, $IFN\gamma$, and **d**, IL-4 ELISpot. **e**, **f**, CD4+ T-cell specific, and **g**, CD8+ T-cell specific cytokine release, determined by flow cytometry. Heights of bars indicate the geometric (a-b) or arithmetic (c-g) means for each group. Whiskers indicate 95% confidence intervals (CI's; a-b) or standard errors of means (SEMs; c-g). Every symbol represents one animal. Horizontal dotted lines mark the LLODs. Values below the LLOD set to ½ the LLOD. Asterisks below the x-axis indicate the day of Dose 2.
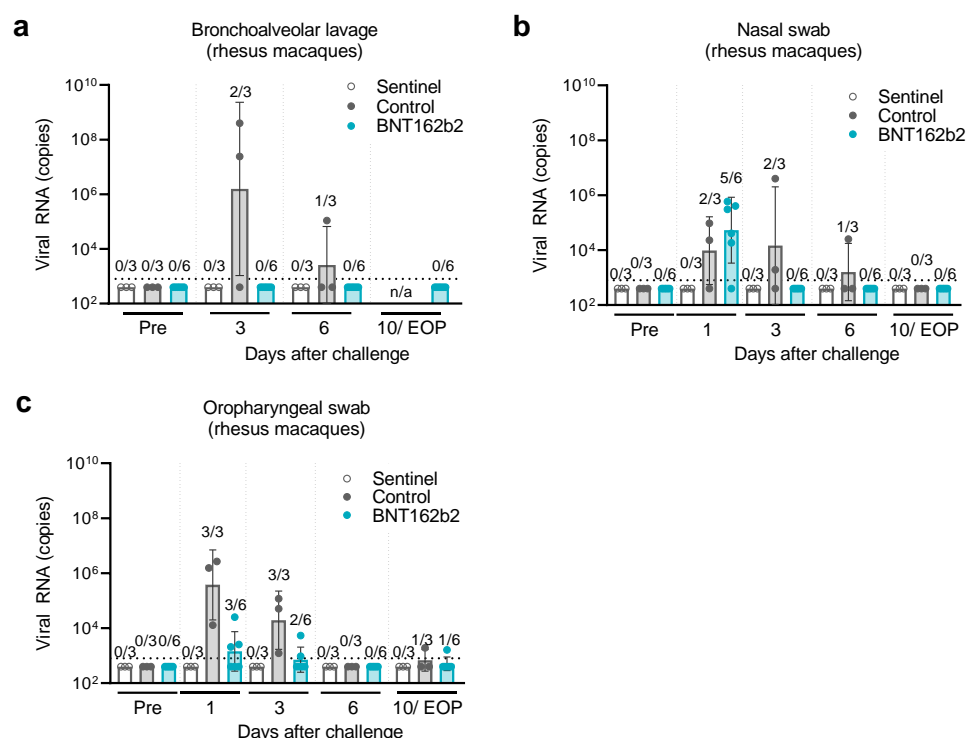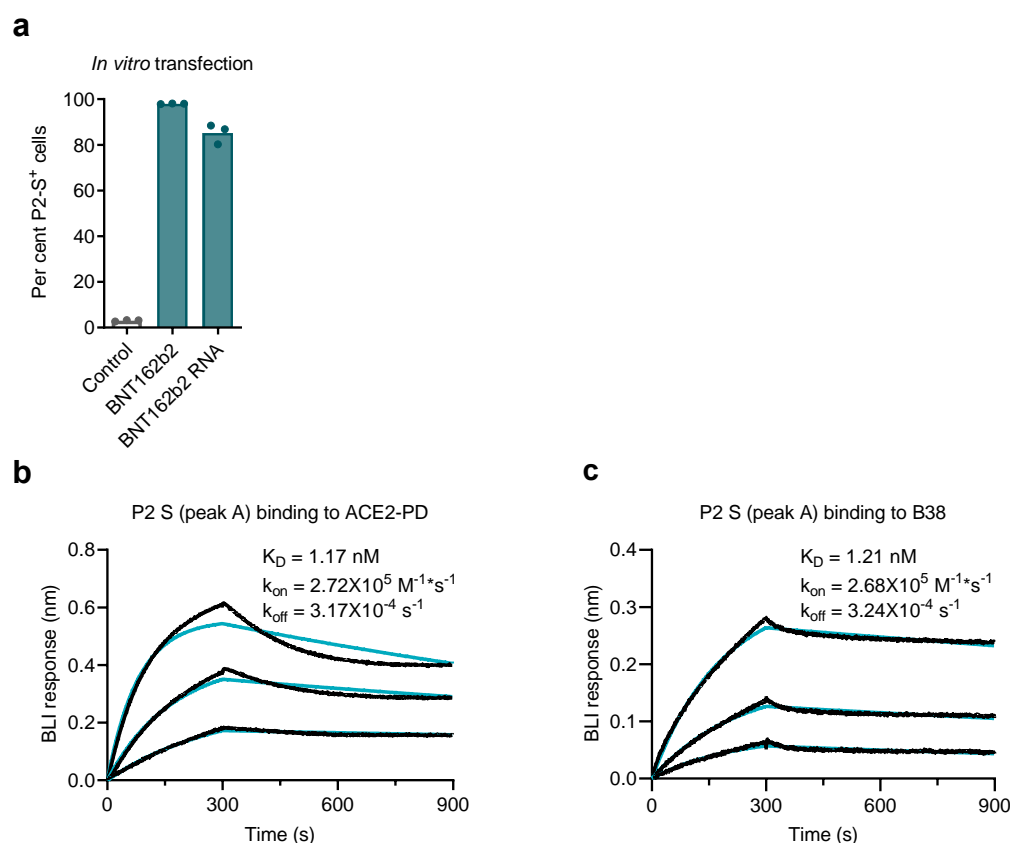
Page 31

Figure 4. Protection of rhesus macaques from challenge with infectious SARS-CoV-2.

Fifty-five days after the Dose 2 of 100 μg BNT162b2 (n=6) or saline control (n=3), rhesus macaques were challenged with 1.05×10^6 total pfu of SARS-CoV-2 split equally between the IN and IT routes. Non-immunised rhesus macaques (n=3) were mock-challenged with cell culture medium (sentinel). Viral RNA levels were detected by RT-qPCR. BAL was performed and nasal and oropharyngeal (OP) swabs obtained at the indicated time points. Final collection of samples was on Day 10 relative to challenge for the sentinel and control groups and at the end of protocol (EOP) on Day 7 or 8 for the BNT162b2-immunised group. Ratios above data points indicate the number of viral RNA positive animals among all animals per group. Heights of bars indicate geometric means. Whiskers indicate geometric standard deviations. Every symbol represents one animal. Dotted lines indicate the lower limits of detection (LLOD). Values below the LLOD were set to ½ the LLOD. **a**, Viral RNA in bronchoalveolar lavage (BAL) fluid. **b**, Viral RNA in nasal swabs. **c**, Viral RNA in OP swabs. The statistical significance by a non-parametric test (Friedman's test) of differences in viral RNA detection between control-immunised and BNT162b2-immunised animals after challenge was p=0.0014 for BAL fluid, p=0.2622 for nasal swabs, and p=0.0007 for OP swabs. n/a – not available.

a

In vitro transfection

b

P2 S (peak A) binding to ACE2-PD

K_D = 1.17 nM
k_{on} = 2.72X10^5 M^{-1}*s^{-1}
k_{off} = 3.17X10^{-4} s^{-1}

c

P2 S (peak A) binding to B38

K_D = 1.21 nM
k_{on} = 2.68X10^5 M^{-1}*s^{-1}
k_{off} = 3.24X10^{-4} s^{-1}

Extended Data Figure 1. P2 S expression and receptor affinity.

a, Fraction of HEK293T/17 cells expressing P2 S determined by flow cytometry after incubation with BNT162b2 RNA formulated as LNP (BNT162b2), BNT162b2 RNA formulated with a transfection reagent (BNT162b2 RNA), or no RNA (Control), determined by flow cytometry. **b, c,** P2 S with a C-terminal TwinStrep tag, expressed in Expi293F cells, was detergent solubilized and purified by affinity and size exclusion chromatography. Protein from the first peak of a size exclusion column, containing intact P2 S and dissociated S1 and S2 fragments, was assayed by biolayer interferometry. Sensorgram of the binding kinetics of TwinStrep-tagged P2 S to immobilised b, human ACE2-PD and c, B38 monoclonal antibody.
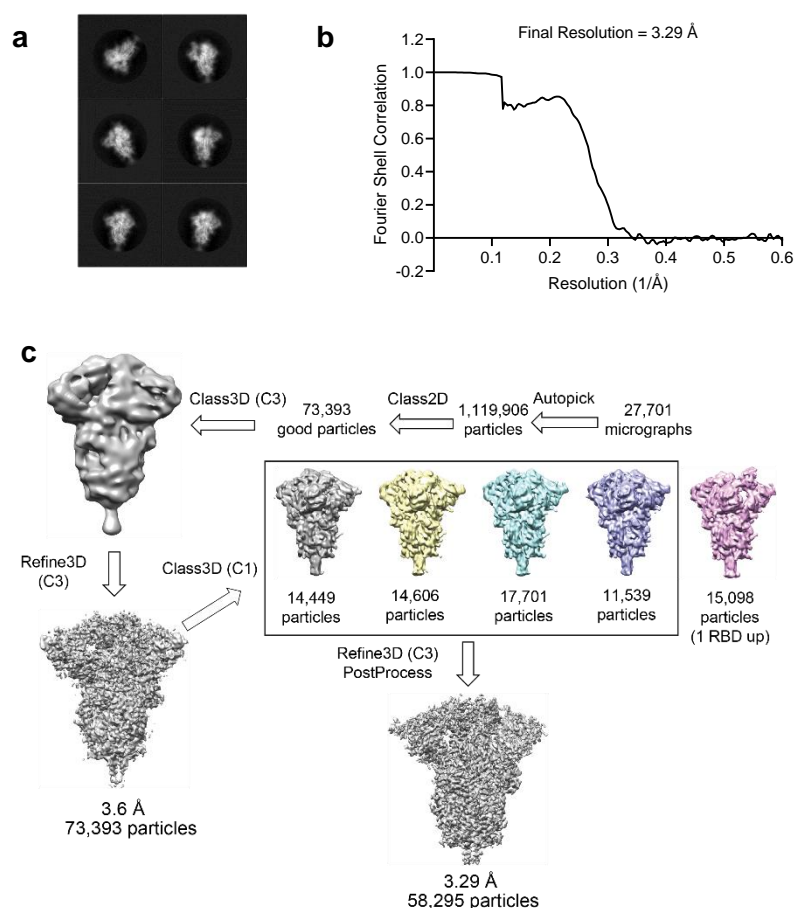
Extended Data Figure 2. Structure analysis of BNT162b2-encoded P2 S by cryo-electron microscopy a, 2D class averages of TwinStrep-tagged P2 S particles extracted from cryo-EM micrographs.. Box edge: 39.2 nm in each dimension. **b**, Fourier shell correlation curve from RELION gold-standard refinement of the P2 S trimer. **c**, Flowchart for cryo-EM data processing of the complex.
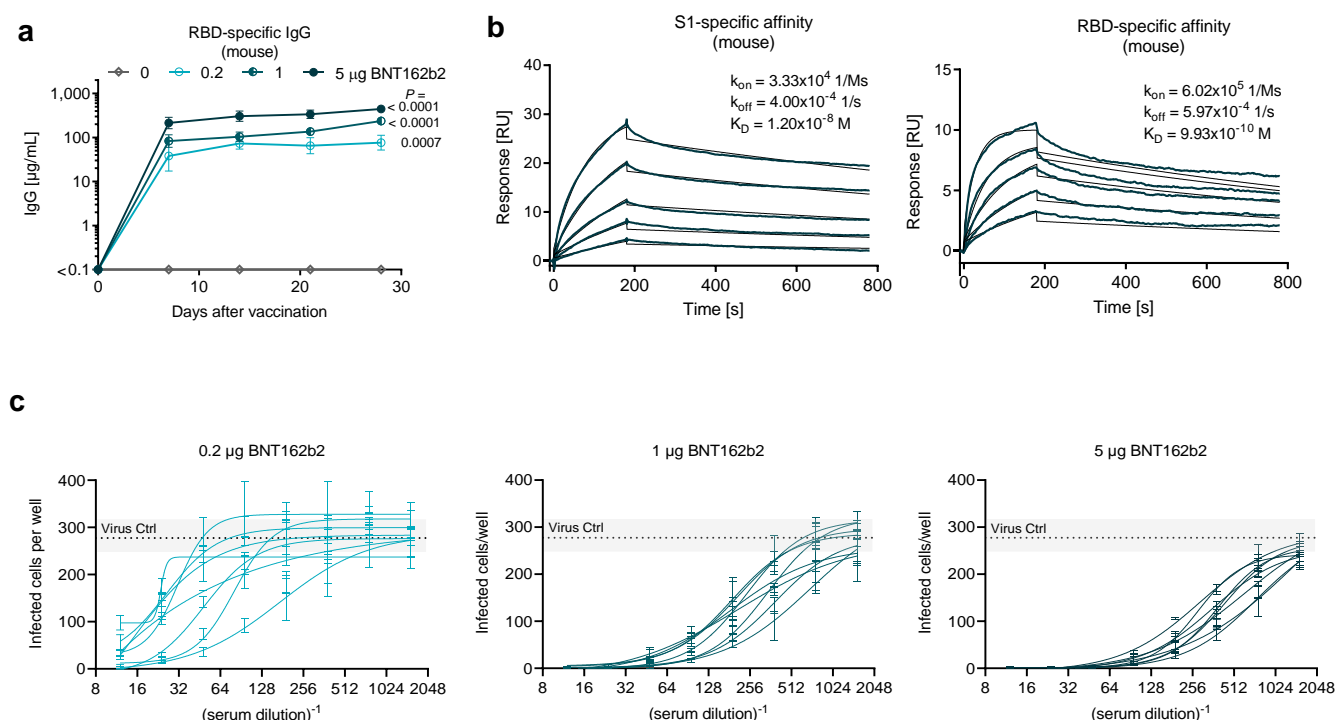
Extended Data Figure 3. BNT162b2-elicited antibody responses in mice.

BALB/c mice (n=8 per group) were immunised intramuscularly (IM) with 0.2, 1 or 5 µg of BNT162b2 or buffer. **a**, RBD-binding IgG responses in sera obtained 7, 14, 21 and 28 days after immunisation, determined by ELISA. For day 0, a pre-screening of randomised animals was performed (n=4). Geometric mean of each group is shown. **b**, Representative surface plasmon resonance sensorgram of the binding kinetics of recombinant S1 *(left)* and RBD *(right)* to immobilised mouse IgG from serum 28 days after immunisation with 5 µg BNT162b2 (n=8). Actual binding (dark blue) and the best fit of the data to a 1:1 binding model (thin line in black). **c**, Number of infected cells per well in pseudovirus neutralisation assays conducted with serially diluted mouse serum samples obtained 28 days after immunisation with BNT162b2 are shown (n=8 per group, see also Figure 2b).
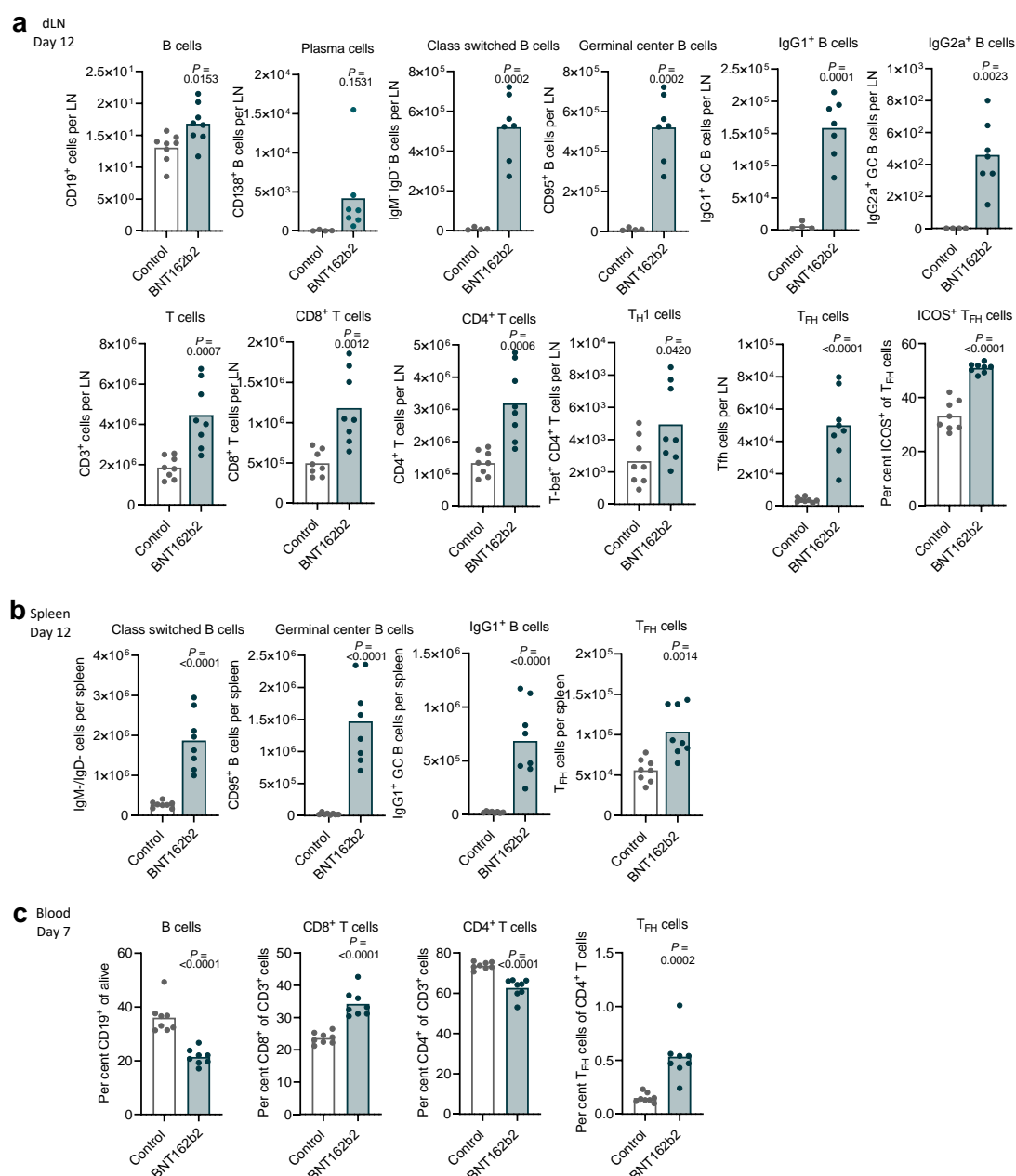
Extended Data Figure 4. B-cell and T-cell phenotyping in lymph nodes, spleen and blood of BNT162b2 immunised mice.

Mice (n=8 per group) were immunised with 5 µg BNT162b2 or buffer (Control). P-values were determined by an unpaired two-tailed t-test. **a**+**b**, B-cell and T-cell numbers 12 days after immunisation in (**a**) draining lymph nodes (dLN; for B-cell subtyping only: n=4 for control, n=7 for BNT162b2 immunised group) or (**b**) the spleen, determined by flow cytometry. The percentage of ICOS$^+$ cells among T follicular helper cells (T$_{FH}$) in dLNs is depicted on the lower right in (a). **c**, B- and T-cell fractions in the blood seven days after immunisation.
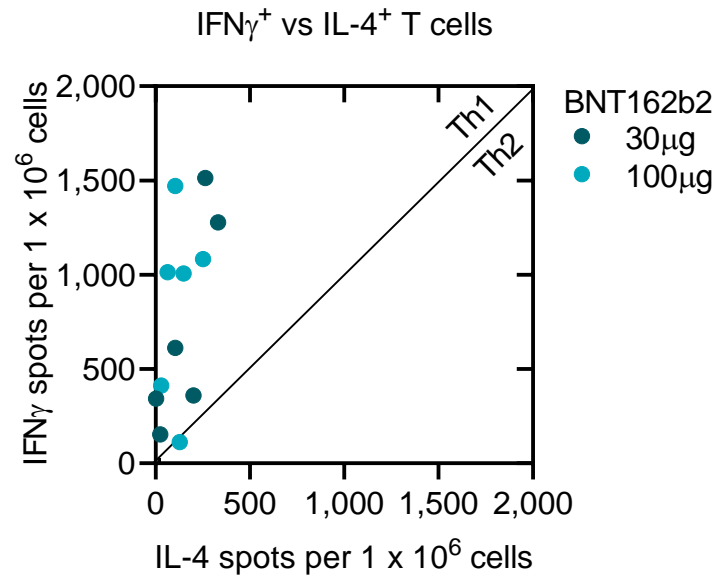
Extended Data Figure 5. Scatterplot of IL-4 vs. IFNγ ELISpot of S peptide stimulated PBMCs collected on Day 42.

Rhesus macaques (n=6 per group) were immunised on Days 0 and 21 with 30 µg or 100 µg BNT162b2 (see Fig. 3c,d) and individual animal values are shown.

Extended Data Table 1. Electron cryomicroscopy data collection, 3D reconstruction and refinement statistics.

Data collection		
EM equipment	Titan Krios (Thermo Fisher Scientific)	
Voltage (keV)	300	
Detector	K2 Summit	
Energy filter	Gatan GIF, 20 eV slit	
Nominal Magnification	165,000 x	
Pixel size (Å)	0.435 (super-resolution)	
	Grid 1	Grid 2
Electron dose ($e^-/Å^2$)	50.32	50.12
Dose rate (e-/Å2/sec)	8.4	8.33
Defocus range (μm)	-1.2 to -3.4	-1.2 to -3.4
Number of collected micrographs	10422	17279
3D Reconstruction		
Software	Warp, Relion	
Number of used particles		
Symmetry imposed	C3	
Global Resolution (Å)		
FSC 0.143	3.29	
Applied B factor ($Å^2$)	-50	
Refinement		
Software	Phenix, Coot	
Protein residues	22,051	
Map Correlation Coefficient	0.82	
RMSD		
Bond length (Å)	0.011	
Bond angles (°)	0.962	
Ramachandran plot statistics (%):		
Preferred	90.4	
Allowed	9.59	
Outlier	0	
Poor Rotamers (%)	11.06	
MolProbity Score	2.96	
Clashscore (all atoms)	13.23	